Analytical and Bioanalytical Chemistry (2021) 413:6627–6637
https://doi.org/10.1007/s00216-021-03629-5

RESEARCH PAPER

A sensitive photothermometric biosensor based on redox reaction-controlled nanoprobe conversion from Prussian blue to Prussian white

Xinyuan Zhang[1,2] · Honghong Rao[2] · Huiyi Huang[1,2] · Kehui Zhang[1] · Mingming Wei[1] · Mingyue Luo[1] · Xin Xue[1] · Zhonghua Xue[1] · Xiaoquan Lu[1]

Received: 3 July 2021 / Revised: 12 August 2021 / Accepted: 19 August 2021 / Published online: 3 September 2021

Abstract

As a new low-cost photothermal nanoprobe, Prussian blue nanoparticles (PB NPs) have been demonstrated to have more potential in photothermometric-based point-of-care testing (POCT) application. However, most of the existing PB NP-based photothermometric sensors were constructed mainly relying on in situ generation of PB NPs or their combination with antigens and antibodies, therefore usually suffering from the inherent defects like complicated preparation and cumbersome surface process as well as high-cost modification. To break this limitation of PB NP-based photothermometric POCT, we proposed an ingenious redox reaction-controlled nanoprobe conversion strategy and successfully applied to photothermometric detection of ascorbate oxidase (AAO). In this design, the heat of PB NP photothermal system under 808-nm laser irradiation dramatically decreased with the addition of AA, due to a unique AA-induced Prussian blue to Prussian white (PB-to-PW) conversion. Upon AAO addition, the heat of reaction system increased because of the enzymatic catalytic reaction between AAO and AA, which led to a significant reduction of AA and resultantly inhibited PB-to-PW conversion. Such target-mediated nanoprobe conversion resulted in an obvious temperature change that could be easily detected by a common thermometer and exhibited good linear ranges from 0.25 to 14 mU/mL with a detection limit as low as 0.21 mU/mL for POCT analysis of AAO. This facile, convenient, and portable photothermometric sensing platform provides an innovative route for the design of PB NP nanoprobe-based photothermometric detection methods.

Keywords Photothermometric · Redox reaction · Prussian blue nanoprobe · Ascorbate oxidase · Point-of-care testing

Introduction

Ascorbic acid (AA, alias vitamin C) is more essential for many biological and chemical processes such as eliminating free radicals, improving immunity, and preventing diseases [1–3]. In clinical practices, AA can be used to relieve vitiligo and reduce the incidence of cancer [4–6]. Ascorbate oxidase (AAO) as a member of multi-copper family [7] can catalyze the oxidation of ascorbic acid to dehydroascorbic acid (DHAA) [8, 9], which usually plays an important physiological role in balancing the level of AA in the human body [10, 11]. Therefore, it is meaningful to establish a simple and sensitive method for point-of-care testing (POCT) AAO activities in human serum for clinical diagnosis and treatment.

Many analytical strategies such as colorimetric and fluorometric have been developed for AAO detection. Li et al. designed a fluorometric biosensor for AAO detection on the basis of fluorescence resonance energy transfer between MoS_2 (MQDs) and CoOOH nanoflakes [12]. Zhang et al. synthesized manganese(II)-doped zinc/germanium oxide nanoparticles (Mn@ZnGe NPs) for colorimetric and fluorometric sensing AA and AAO [13]. However, these methods

✉ Honghong Rao
rhh@nwnu.edu.cn

✉ Zhonghua Xue
xzh@nwnu.edu.cn

[1] Key Laboratory of Bioelectrochemistry & Environmental Analysis of Gansu Province, College of Chemistry & Chemical Engineering, Northwest Normal University, Lanzhou 730070, China

[2] College of Chemistry & Chemical Engineering, Lanzhou City University, Lanzhou 730070, China

usually were developed, relying on the complicated preparation processes of nanoprobe as well as bulky and expensive instruments. It is therefore an urgent need for developing novel detection technologies with simple, convenient yet high sensitivity and selectivity to answer point-of-care testing AAO especially in low-resource settings.

In recent years, photothermometric assays have attracted great attention in POCT due to its simple operation process and easy to detect signal readout [14–16]. In a photothermometric detection event, the sensing readout of temperature change could be easily detected via a widely used thermometer relying on the use of photothermal probe under near-infrared (NIR) irradiation [17–19]. Many of photothermal agents and nanomaterials as the potential photothermal nanoprobe have been explored in the field of photothermometric POCT such as Au nanostructures [20, 21], carbon-based materials [22, 23], copper chalcogenide semiconductors [24, 25], and organic dye molecules [26, 27]. Among them, Prussian blue nanoparticles (PB NPs) have been demonstrated to be more potential in photothermometric sensing application due to their good photothermal effect [28, 29]. More importantly, PB NPs as an ancient dye exhibited more advantages such as low cost, easy preparation, and higher molar extinction coefficient [30–32]; especially, it has been approved in clinic for treatment of radioactive exposure by the U.S. Food and Drug Administration (FDA) due to its outstanding biosafety [33]. Taking the above benefits of PB NPs, lots of efforts have been made to advance the development of PB NP-based photothermometric detection methods. For example, Li et al. develop a photothermal microfluidic sensing platform by using analyte-mediated PB NP photothermal nanoprobe to quantitatively sense Ag^+ [34]. Our group explored a bimodal method for photothermometric and colorimetric detection of Fe^{3+} based on an in situ PB NP nanoprobe generation strategy [35]. But most of the existing PB NP-based photothermometric sensors were constructed mainly relying on in situ generation of PB NPs [32, 36] or the direct use of PB NP photothermal nanoprobe with the combination of some antigens and antibodies [37, 38], therefore usually suffering from the inherent defects like complicated preparation and cumbersome surface process as well as high-cost modification. Therefore, it is very important to explore a simple, effective, and portable strategy for advancing the development of PB NP-based photothermometric POCT.

Herein, we communicate that AA can exceptionally induce PB NPs to Prussian white (PW) conversion and further lead to a distinct photothermal signal change, allowing us to design a simple, portable, and sensitive photothermometric assay for AAO detection. In this design, PB NPs as the effective photothermal probe can absorb light upon 808-nm NIR irradiation and convert it into heat with a significant temperature increase (Scheme 1). However, AA can exclusively induce a PB-to-PW conversion accompanying with a significant photothermal change response. Upon AAO addition, such photothermal nanoprobe conversion was inhibited greatly due to the enzymatic catalytic reaction between AAO and AA, finally enabling us to photothermometric sensing AAO in the solution system.

Material and methods

Materials and regents

Ascorbate oxidase (AAO), glucose oxidase (GO_x), uricase (UAO), alkaline phosphatase (ALP), hyaluronidase (HAase), trypsin (Try), lysozyme (Lyz), bovine serum albumin (BSA), glutathione (GSH), cysteine (Cys), and $FeCl_3$ were purchased from Sigma-Aldrich Co. Ltd. (Shanghai, China). Ascorbic acid (AA), citric acid, Na_2HPO_4, NaH_2PO_4, and $K_4[Fe(CN)_6]$ were obtained from Shanghai Zhongqin Chemical Reagent Co. Ltd. (Shanghai, China). All reagents were of analytical grade and were used without any further purification. Aqueous solutions were prepared with deionized water (18.24 MΩ cm).

Instrumentation

The UV-vis absorption spectra were measured using a T6 new century spectrophotometer (China). A diode laser (MDL-H-808-5W-17120005) was purchased from Changchun New Industries Optoelectronics Technology Co. Ltd with a tunable output power from 0 to 5 W. Transmission electron microscopy (TEM) was performed on FEI electron microscopy (TECNAI, G2 F20 S-TWIN, US) equipped with an energy-dispersive X-ray spectroscopy (EDX) (Gatan 832) operating at an accelerating voltage of 200 kV. X-ray photoelectron spectroscopy (XPS) was performed by using an ESCALAB 250Xi (ThermoFisher Scientific, USA). Fourier transform infrared (FTIR) spectra measurements were obtained on a FTS3000 Fourier transform infrared spectrometer (DIGI-LAB, USA). Roman spectra was obtained from HORIBA Jobin Yvon S.A.S. Roman spectrometer (LabRAM HR Evolution, French). The real pH value of different buffer solutions was measured by a Metrohm 632 pH meter. Centrifugation was performed on a Ke Cheng H3-18K centrifuge. Constant warm water bath (Jing Hong DK-S24, China) was employed for incubating enzyme. A pen-style digital thermometer (model number MITIR-TP677) was obtained from a local supermarket (detection range of −50 to +300 °C). All photographs were recorded by a Canon camera (EOS-70D, Japan). Temperature detection of AAO on filter paper was done using an IR Thermal Imager (FLIR C2, American).

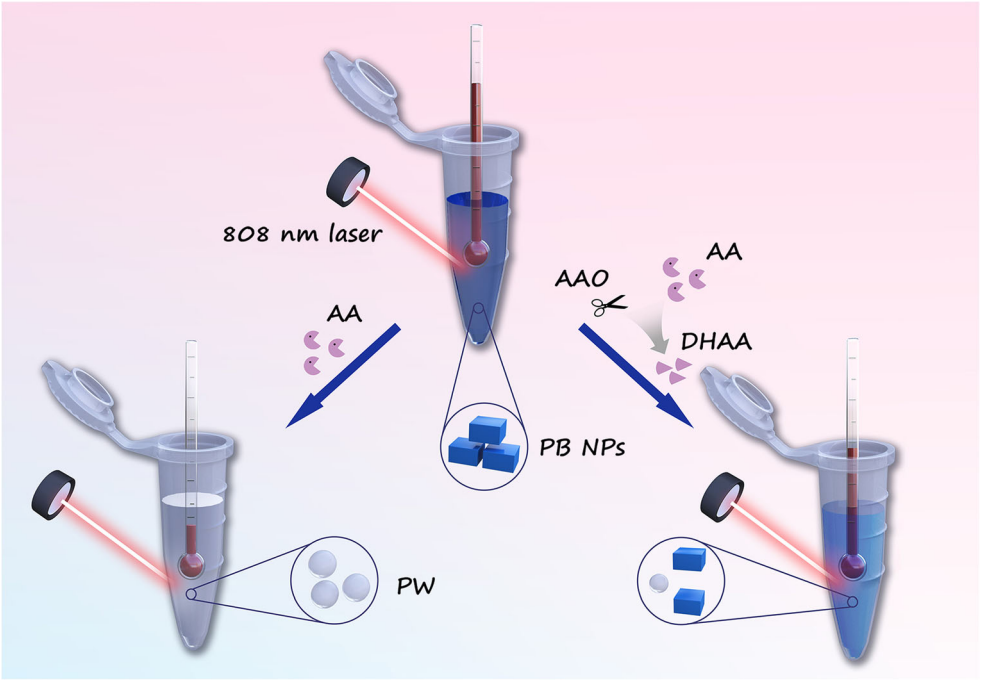

Scheme 1 Schematic illustration of the proposed photothermometric sensing principles toward AAO based on the redox reaction-controlled nanoprobe conversion strategy

Synthesis of PB NPs

PB NPs were prepared according to the previously reported method [39]. In detail, two homogeneous solutions were initially prepared: solution A contains 1 mM $K_4[Fe(CN)_6]$ and 1 mM citric acid, which was preheated to 60 °C; solution B contains 1 mM $FeCl_3$ and 1 mM citric acid. These two solutions were mixed at 60 °C under vigorous stirring for 30 min. Then, the resultant suspension was naturally cooled at room temperature and centrifuged at 10000 rpm for 30 min. After that, the collected precipitates were washed with deionized water for several times. Finally, the products were dried at 60 °C in an oven and redispersed in deionized water and stored at 4 °C.

Photothermometric detection of AAO

Firstly, 14 μL AAO with different concentrations and 16 μL of AA (10 mM) were added into 1910 μL of PBS buffer solution (0.2 M, pH 7.0) and incubation at 37 °C for 60 min. Then, 60 μL of PB NPs (1 mM) was added into the mixed solutions in the reaction tubes (total volume 2 mL) and reacted at room temperature for 10 min. After that, the UV-vis spectra of the reaction solution were subsequently recorded using a UV-vis spectrophotometer and the corresponding photograph was taken by using a digital camera. The standard curve of the colorimetric assay was established according to the equation $\Delta A = A_1 - A_0$, in which ΔA is the absorbance change of the PB NPs nanoprobe at 700 nm and A_0 and A_1 represent the absorbance values in the absence and presence of AAO, respectively. For the photothermometric testing, the cuvettes of the above reaction solutions were irradiated horizontally with an 808-nm laser at a power of 4.5 W for 210 s. Meantime, a pen-style digital thermometer was inserted in the reaction solution to monitor the temperature increase during the irradiation process. Herein, the standard curve of photothermometric assay was established according to the equation ΔT (°C) = $\Delta T_1 - \Delta T_0$, where ΔT refers to the temperature variation, ΔT_0 represents the temperature increase before and after irradiation in the absence of AAO, and ΔT_1 represents the temperature increase before and after irradiation in the presence of AAO, respectively. To measure the uniform temperature of the solution, a small magnet in the cuvette was always stirred at a speed of 800 rpm during the irradiation experiment process.

Human serum sample detection

To evaluate the accuracy of the proposed colorimetric and photothermometric method, the level of AAO in human serum was detected by using the standard addition method. For this purpose, diluted human serum solutions (1%) were spiked with 1, 5, and 10 mU/mL AAO, respectively. Then, 14 μL of the spiked human serum samples was mixed with 16 μL of AA (10 mM) into 1910 μL PBS buffer solutions (0.2 M, pH 7.0) and then incubated at 37 °C for 60 min. Subsequently, 60 μL of 1 mM PB NPs was added into the mixed solutions. Finally, the samples were submitted to the same colorimetric and photothermometric analysis by using the method described above. Human serum specimens were derived from Hospital 940 of PLA Joint Logistics Support Force, Lanzhou, China. Here, we state that all experiments were performed in accordance with the Guidelines on

Administration of Lab, and approved by the ethics committee at Northwest Normal University.

Results and discussion

Characterization of PB NPs

PB NPs were prepared using a typical wet synthesis strategy according to the previously developed method as illustrated in Fig. 1a. The obtained PB NPs appeared to be typical cube particles of ~40 nm under TEM (Fig. 1b) and exhibited a broad band spectrum with a maximum absorption peak at 700 nm in UV-vis spectrum along with a distinct blue color (Fig. 1c and inset) [40]. The elements of obtained PB NPs were confirmed by energy-dispersive X-ray spectroscopy (EDX) which suggests the presence of Fe, C, and N elements (Fig. 1d) [41]. X-ray photoelectron spectroscopy (XPS) was further used to confirm the formation of PB NPs product. Two characteristic peaks located at 708.7 and 721.6 eV corresponding to the existence of Fe^{II} and 712.8 and 724.5 eV attributing to the presence of Fe^{III} in the obtained PB NPs were clearly displayed [42] (Fig. 1e). Furthermore, FTIR spectra show a sharp peak at 2085 cm^{-1} attributing to the stretching region of C≡N (Fig. 1f) [32] and Raman spectra display an intense and sharp band at about 2156 cm^{-1} corresponding to

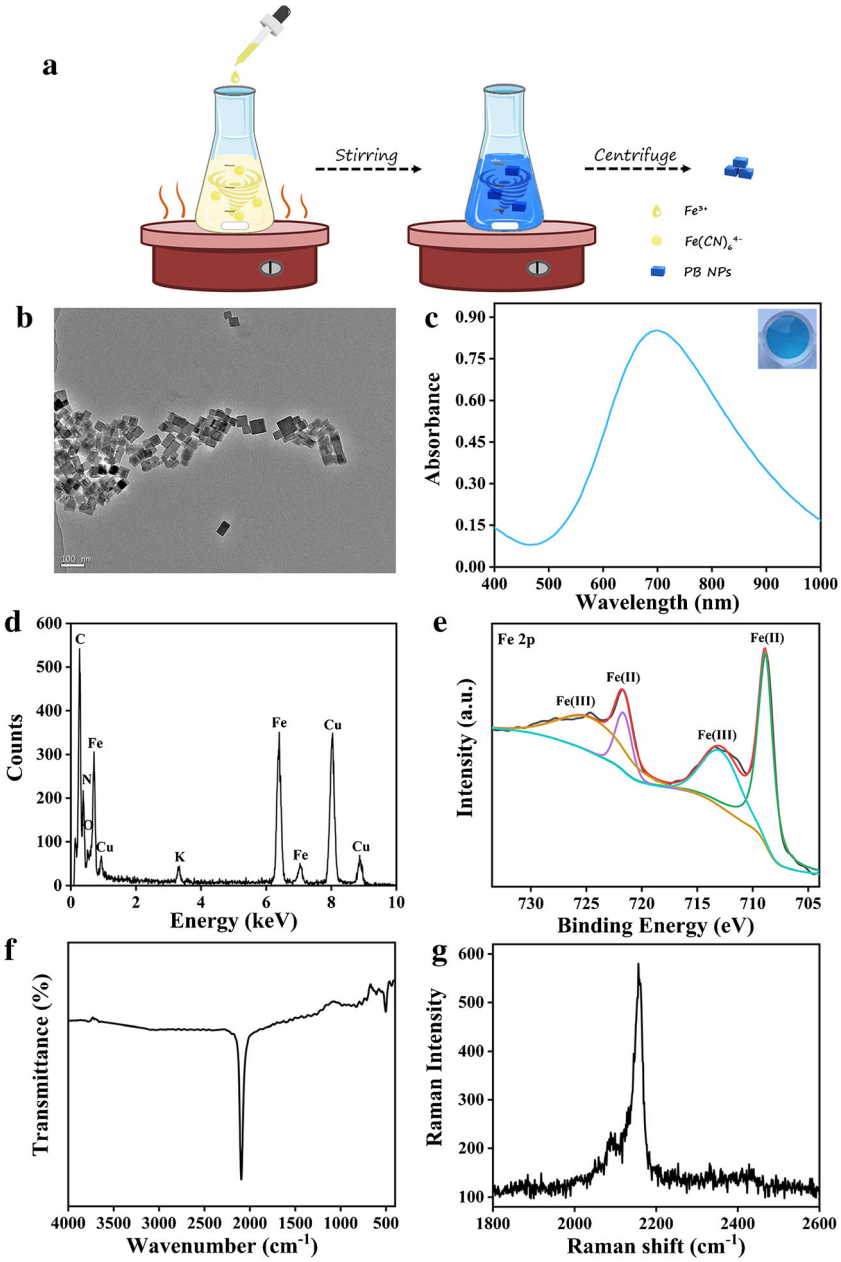

Fig. 1 (a) Schematic illustration of synthesis of PB NPs; (b) TEM images, (c) UV-vis absorption spectra (inset: the corresponding photograph), (d) EDS spectrum, (e) Core-level Fe 2p XPS profiles, (f) FTIR spectra, (g) Raman spectra of PB NPs

the stretching vibrations of cyanide groups (CNs) that coordinated with ferric ion (Fig. 1g) [29]. All of the above observations strongly indicate the successful preparation of PB NPs.

Photothermometric effects of the proposed photothermometric AAO sensor

To study the feasibility of the target (AAO)-mediated nanoprobe conversion system for AAO sensing with colorimetric and photothermometric readout, we first evaluated the optical, colorimetric, and photothermometric properties of the system upon different components. As illustrated in Fig. 2a, we speculated that AA might sensitively induce a PB-to-PW conversion and therefore exhibit a significant colorimetric and photothermometric response. Upon AAO addition, such nanoprobe conversion was inhibited greatly due to the enzymatic catalytic reaction between AAO and AA. To verify this hypothesis, the photographs, UV-vis spectra, and the 808-nm laser-driven photothermal effect of different reaction systems were recorded. We utilized $\Delta T'$, that is, $\Delta T' = T - T_r$, as the photothermal measurement signal for each sample solution, where T_r is a stable temperature value before irradiation and T is the temperature value after 210-s irradiation. As shown in Fig. 2b, the system containing PB NPs displays an intense blue color (Fig. 2b, insert c) along with a dramatic UV-vis absorption peak around 700 nm (Fig. 2c, green curve) that corresponds to the characteristic optical property of PB NPs [40]. However, an intense blue to pale blue color change (Fig. 2b, insert f) and a dramatical decrease on the absorbance of ~700 nm (Fig. 2c, red curve) were observed for PB NPs system in the presence of AA (80 μM) at given conditions, indicating an obvious AA-induced PB-to-PW conversion process consistent with the previous reports [43, 44]. Significantly, an obvious color change from pale blue to intense blue (Fig. 2b, insert g) and a dramatical UV-vis absorption increase (Fig. 2c, navy blue curve) were observed only in the presence of PB NPs, AA, and AAO, whereas no apparent color change and absorbance were exhibited in other cases. It may be attributed to the specific enzymatic catalytic reaction between AAO and AA [10], which results in a great inhibition on the PB NP nanoprobe conversion. These results strongly indicate the possibility of our system for colorimetric sensing AAO activity. Furthermore, we also found that our redox reaction-controlled nanoprobe conversion system could not only provide the sensitive colorimetric signal readout, but also present a potential photothermometric signal readout. It is worth noting that PB NPs exhibit a significant light absorption in the NIR region (Fig. 2c, green curve), thus showing a great promise for developing a photothermometric sensing platform. Therefore, different component-based colorimetric reaction systems were exposed to an 808-nm laser at a power of 4.5 W for 210 s to test the photothermal effect of the reaction system. Using a pen-style digital thermometer, the temperature of the different solution systems was measured in the irradiation process. As clearly shown in Fig. 2d, a dramatic temperature increase of 28.5 °C correspondings to PB NP photothermal conversion was observed for the blue-colored PB NP colorimetric solution. With the addition of AA, only an apparently decreased temperature increase of 6.7 °C was observed for PB NP-AA system. Interestingly, with the further

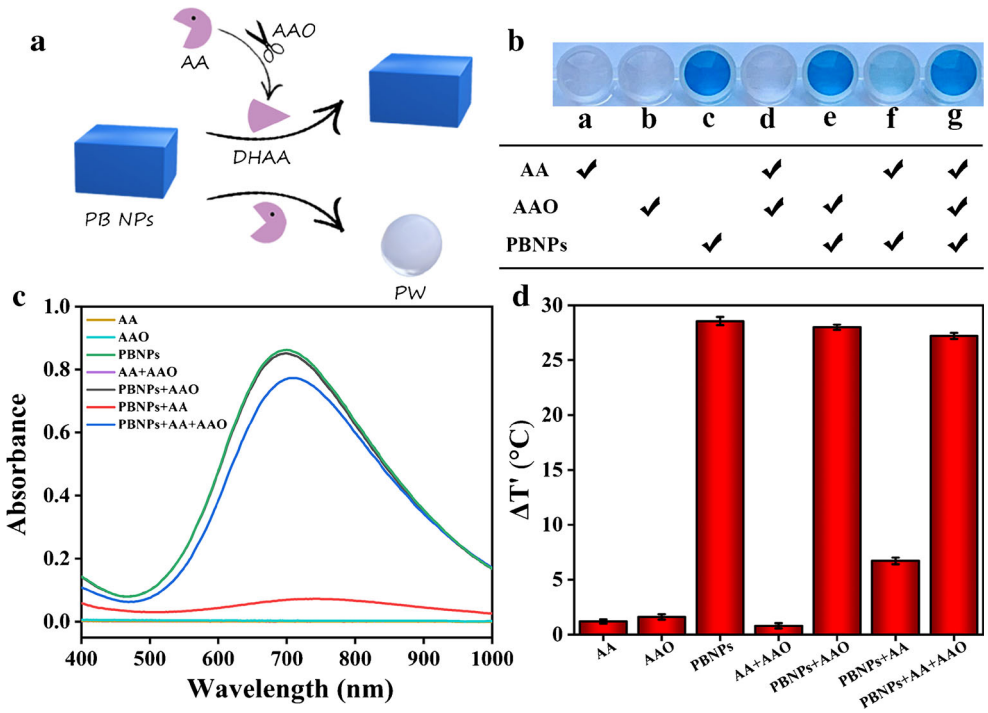

Fig. 2 Feasibility of the proposed redox reaction-controlled nanoprobe conversion strategy. (a) Schematic diagram of AAO induced signal indicator; (b) photographs, (c) UV-vis absorption spectra, and (d) temperature increases ($\Delta T'$) of the reaction systems with different components. The final concentrations of AA, AAO, and PB NPs are 80 μM, 14 mU/mL, and 30 μM, respectively. Error bars indicate standard deviations ($n = 3$)

addition of AAO, PB NP-AA system then demonstrated an obvious temperature increase (~ 27.2 °C), while no significant temperature increases were recorded in other cases. Such observation accordingly demonstrates that our proposed redox reaction-controlled nanoprobe conversion system presents a sensitive photothermometric response toward AAO, and therefore may be used to build a photothermometric detection method for AAO activity.

To further confirm the colorimetric and photothermometric performance of our redox reaction-controlled nanoprobe conversion system, the response of the corresponding color, UV-vis absorption, and temperature increase of the proposed colorimetric and photothermometric reaction system toward different AAO contents were further investigated. With the increasing AAO concentrations (1, 5, 10 mU/mL), a gradual color change from pale blue to blue with a distinct AAO content-dependent feature can be clearly observed (inset of Fig. 3a). Additionally, such observed color response also demonstrates a gradual increasing tendency in the UV-vis absorbance. Figure 3a displays an increased absorption in the UV-vis spectra centered at 700 nm closely linked with the change of AAO content, suggesting a closely AAO content-dependent PB NP nanoprobe conversion. In addition, the colorimetric reaction system with different AAO concentrations exhibits a different photothermometric response upon 808-nm laser irradiation for 400 s at a power of 4.5 W (Fig. 3b). Specifically, AAO with high concentration correspondingly gives the maximal enhanced temperature for the proposed redox reaction-controlled nanoprobe conversion system. Such observation further indicates the possibility of this proposed PB NP system for photothermometric detecting AAO activity through a simple redox reaction-controlled nanoprobe conversion strategy. Moreover, the reaction process was further confirmed by TEM as shown in Fig. S1 in the Supplementary Information. Obviously, PB NPs with typical cube shape almost disappeared in the absence of AAO but presence of 80 μM AA at given reaction condition, indicating that AA successfully induced the morphological evolution of PB NPs (Fig. S1a). Such cube appearance to sphere-like shape transformation of PB NPs was gradually hindered with the increasing AAO concentrations (Fig. S1b, c, and d). All these results indicate that the PB NPs to PW morphological evolution is obviously dependent on the enzymatic catalytic reaction between AA and AAO as well as the unique reaction between AA and PB NPs. Further proofs were also obtained by XPS spectra and FTIR spectra (Fig. S2). As shown in Fig. S2a, PB NPs showed the mixed valences of iron containing typical Fe^{II} characteristic peaks (708.7 and 721.6 eV) and Fe^{III} characteristic peaks (712.8 and 724.5 eV). As a comparison, all four of characteristic peaks show a significantly decreased tendency upon the addition of AA. Moreover, the FTIR spectrum (Fig. S2b) also showed that the characteristic peak of PB NPs at 2085 cm^{-1} of the C≡N stretching region was disappeared after AA addition. All these results strongly indicate that AA can effectively induce a PB-to-PW conversion.

Optimization of AAO detection conditions

To obtain an excellent detection performance toward AAO analysis, some key factors that influenced the sensing results such as concentrations of AA, pH, incubation time, reaction time, the laser irradiation power, and time were optimized in detail. Firstly, the concentration of AA was optimized by investigating the characteristic absorbance of PB NPs at 700 nm (A_{700}) of PB NP reaction system upon the addition of different AA contents from 10 to 100 μM. As shown in Fig. S3a, with the increment of AA concentration over the range of 10–100 μM, the value of A_{700} gradually decreased and reached a plateau at 80 μM of AA. Thus, the optimal AA concentration of 80 μM was selected in the subsequent experiments. Secondly, the optical change of characteristic absorbance of PB NPs at 700 nm (ΔA_{700}) in UV-vis spectra was proposed as the criterion to investigate the influence of the above-mentioned conditions. The effect of our reaction system in the PBS buffer solution with different pH values is shown in Fig. S3b. The obtained ΔA_{700} reaches a maximum as the pH value located at 7.0, and thus, pH 7.0 was selected as the optimal pH in the subsequent experiment. Subsequently, we tested the effect of incubation time; the characteristic ΔA_{700} increased gradually first with the increasing incubation time of

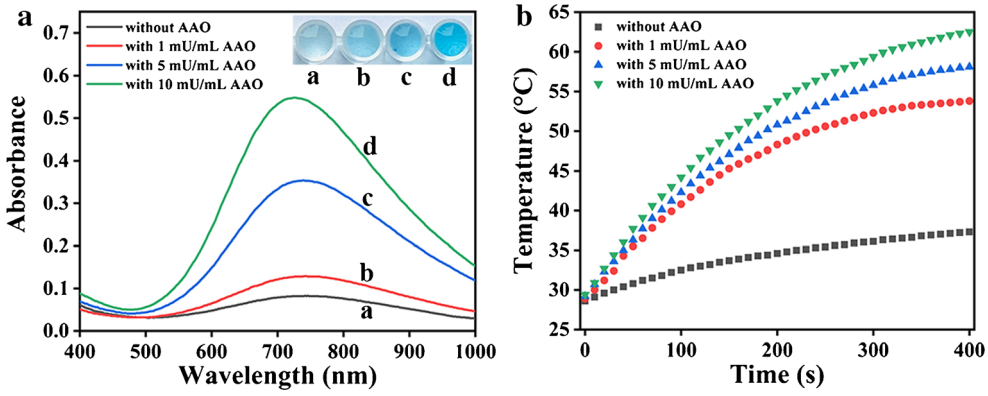

Fig. 3 (a) UV-vis absorption spectra and (b) temperature changes of the reaction solution system without and with 1 mU/mL, 5 mU/mL, and 10 mU/mL AAO. Inset: Photographs of the corresponding solutions under visible light

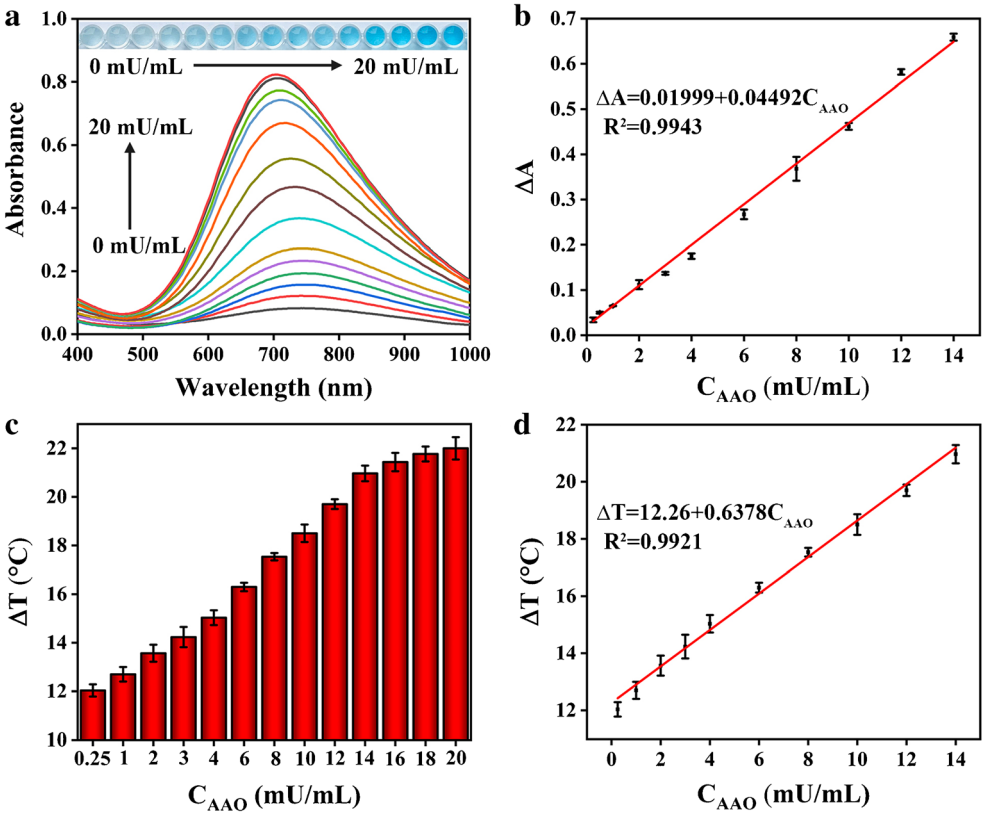

Fig. 4 (a) UV-vis absorption spectra of reaction system with different concentrations of AAO in the range from 0 to 20 mU/mL. Inset: Photographs of the corresponding solution. (b) Calibration plots of absorbance changes (ΔA) of the proposed reaction system vs the different concentrations of AAO. (c) Histogram of the temperature increase (ΔT) of the proposed reaction system with different concentrations of AAO under the irradiation of an 808-nm laser at 4.5 W for 210 s. (d) Calibration plots of temperature increase (ΔT) of the proposed reaction system vs the different concentrations of AAO. Error bars indicate standard deviations (n = 3)

AAO and AA and then gradually stabilized after 60 min (Fig. S3c). So, 60 min as the optimal incubation time was selected for the subsequent study. Following this procedure, the influence of reaction time was also optimized. It is clear that the value of ΔA_{700} showed a continual decrease with the increasing of reaction time (Fig. S3d), demonstrating a significant time-dependent absorbance response. Considering time-saving and the practical application of our analysis platform, 10 min as the optimal reaction time was selected.

Usually, the laser irradiation power and irradiation time of near infrared (NIR) play key roles as the important influencing factors of the photothermal effect in the photothermometric system. Hence, the influences of the laser irradiation power and irradiation time on the photothermal effect of our proposed reaction system were investigated in detail. As shown in Fig. S4a, the temperature of the reaction system increased dramatically with increasing irradiation power of the 808-nm laser and presented a slowly rising trend at a power of 4.5 W. Therefore, 4.5 W as the optimal irradiation power was chosen for the investigation of photothermometric detection. In addition, the influence of the irradiation time of an 808-nm laser on the photothermometric response was also studied, as shown in Fig. S4b. As the PB NP concentration increased, the temperature of the reaction system increased significantly for the same irradiation time from 30 to 240 s. More significantly, we also found such obtained temperature increase (ΔT) exhibited a good linear relationship with PB NP concentration in the range from 10 to 30 μM and with a highest slope at 210 s (0.5784, along with an R^2 of 0.9955) (shown in Table S1), which is more useful for fabricating thermometer readout-

Table 1 Comparison of the sensing performance of the different methods on AAO detection

Detection methods	Material	Linear range (mU/mL)	LOD (mU/mL)	Ref.
Fluorescent	Papain-capped Au/Ag NCs	5–80	1.72	[10]
Colorimetric	DNA-Au/Ag NCs	10–200	6.8	[11]
Fluorescent		10–200	4.8	
Fluorescent	MoS_2 MQDs	2–40	0.8	[12]
Phosphorescent	Mn@ZnGe NPs	1000–4000	850	[13]
Fluorescent		1250–2500	728	
Photothermometric	PB NPs	0.25–14	0.21	This work

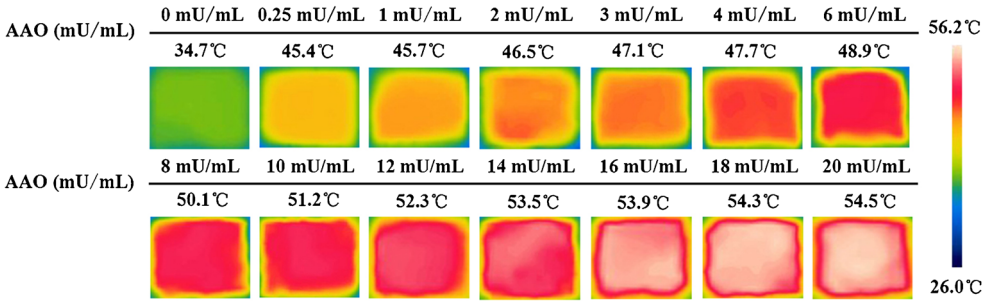

Fig. 5 IR images showing the temperatures of test paper with different concentrations of AAO (0–20 mU/mL) under 808-nm laser irradiation at a power of 4.5 W for 210 s

based quantitative strategy due to the sensitive photothermal signal than other cases. Thus, 210 s was used as the optimal irradiation time in the subsequent study.

Photothermometric detecting AAO

Under the optimum conditions, the photothermometric detection of AAO was achieved by simply monitoring the temperature variation of the reaction system through a common thermometer. Different concentrations of AAO varying from 0 to approximately 20 mU/mL were added into the sensing system. With the increasing AAO concentration, the typical absorption peak of PB NPs at 700 nm increased gradually (Fig. 4a), and simultaneously, the solution color changed from pale blue to blue color (inset of Fig. 4a). In addition, it is worth noting that the ΔA_{700} was increased linearly in the AAO concentration from 0.25 to 14 mU/mL, and was determined as $\Delta A = 0.01999 + 0.04492C_{AAO}$ with R^2 of 0.9943, indicating good colorimetric feasibility of the proposed sensing system for the quantitative AAO analysis. However, the requirement of a spectrometer in the colorimetric method is necessary and therefore represents a huge hindrance for POCT of AAO. We therefore investigated the photothermometric sensing performance of this platform for the quantitative detection of AAO by using a simple temperature readout with a common thermometer reader.

For photothermometric AAO analysis, the system with different concentrations of AAO was irradiated with an 808-nm laser for 210 s at the power of 4.5 W. As displayed in Fig. 4c, the system temperature gradually increased with increasing AAO content in the range from 0.25 to 20 mU/mL. More significantly, a favorable linear correlation between temperature increase (ΔT) and concentration of AAO could be available ranging from 0.25 to 14 mU/mL, which could be fitted to ΔT (°C) = 12.26 + 0.6378C_{AAO} (R^2 = 0.9921) (Fig. 4d). Based on this observation, the limit of detection (LOD) of our photothermometric method for AAO detection was estimated to be 0.21 mU/mL (3δ/K). In addition, we compared the sensing performance of the proposed photothermometric method with other existing AAO detection methods (Table 1). It is clear that our PB NP nanoprobe-based photothermometric method is more sensitive for AAO sensing compared with some reported methods. In addition, it is simple, rapid, convenient, and economical through employing a common thermometer as a simple reader, whereas conventional quantitative methods require expensive instruments.

In order to further improve our photothermometric assay for instantly on-site detection of AAO activity, we provide a simple strategy for converting the photothermal response from

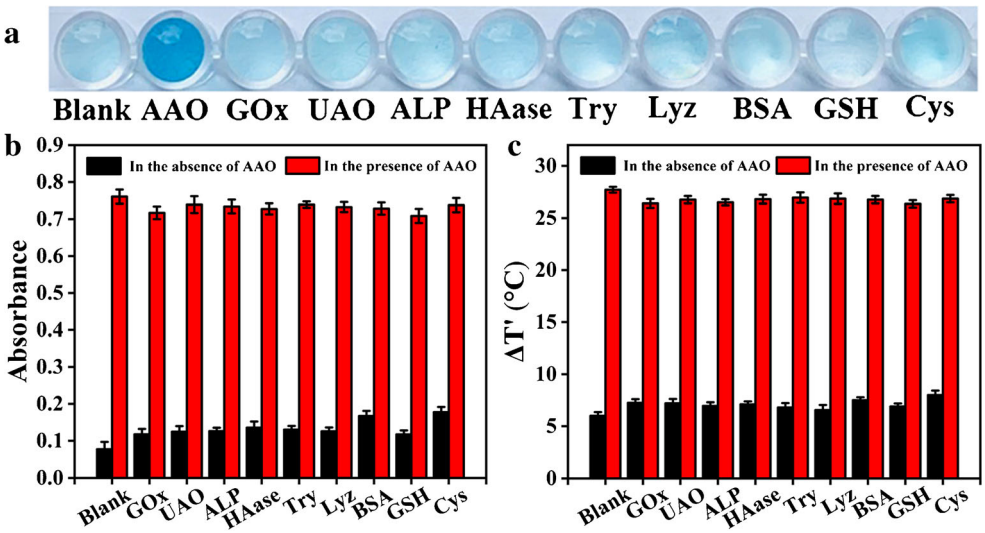

Fig. 6 (a) Photographs, (b) histogram at 700 nm from the UV-visible absorption spectra, and (c) temperature increases ($\Delta T'$) of the reaction system in the absence (black columns) and presence (red columns) of AAO with the addition of different control interfering biomolecules. (The final concentration of AAO is 14 mU/mL, and all interfering substances are at 20-fold higher concentrations than AAO.) Error bars indicate standard deviations (n = 3)

Table 2 Determination results of AAO in the human serum

	Spiked (mU/mL)	Found (mU/mL)	Recovery (%)	RSD (%)
Colorimetric	0	—	—	—
	1	1.03	103.0	6.33
	5	5.14	102.8	3.81
	10	9.75	97.5	5.19
Photothermometric	0	—	—	—
	1	1.02	102.0	5.84
	5	5.03	100.6	3.61
	10	9.76	97.6	7.13

the liquid-phase system on a test paper, allowing an IR thermal imager-based analysis. For the detection of AAO, the reaction solution system with different concentrations of AAO was dropped on a common filter paper (1 cm × 1 cm). Subsequently, we measured the temperature of filter using an IR thermal imager after 210 s of illumination at an 808-nm laser, finally enabling a simple and visual analysis of AAO activity. As shown in Fig. 5, as the concentration of AAO increased, the infrared thermal image captured by an infrared thermal imager gradually changed from yellowish-green to white, indicating that the temperature of the test paper gradually increased. This observation strongly demonstrated that the test paper based on our redox reaction-controlled nanoprobe conversion system has a potentiality for application to instant analysis of AAO activity.

Selectivity of the proposed strategy toward AAO sensor

To evaluate the selectivity and interference resistance of our redox reaction-controlled nanoprobe conversion system for AAO detection, some interfering biomolecules such as GOx, UAO, ALP, HAase, Try, Lyz, BSA, GSH, and Cys with 20-fold higher concentrations than target AAO were added into the reaction system to investigate the colorimetric and photothermometric performance of our sensing system. As clearly shown in Fig. 6a, only target AAO leads to the sensitive pale blue to intense blue color change, along with a significant increase in the characteristic UV-vis absorbance of A_{700} (Fig. 6b and Fig. S6) and a distinct NIR-driven temperature increase (Fig. 6c), whereas no significant color, absorbance, or temperature increase was observed for the added interferents. More significantly, it is clear that no obvious absorbance responses and photothermal responses were observed to colorimetric and photothermometric AAO sensing after the addition of other interfering biomolecules. All these results reveal that our proposed system has an excellent selectivity and specificity toward AAO determination.

In addition, in order to evaluate the effect of laser irradiation on enzyme activity, we measured the characteristic absorbance of the reaction system before and after irradiation. As shown in Fig. S7, with the gradual increase of irradiation time and temperature, the characteristic absorption peak of the proposed photothermometric system at 700 nm had no obvious change, indicating that long time laser irradiation had little effect on enzyme activity as well as the determination of AAO.

Detection of AAO in human serum

Aiming to validate the potential applicability of our developed colorimetric and photothermometric detection method, AAO with different concentrations were spiked into the diluted human serum sample for recovery tests. As listed in Table 2, the obtained recoveries varied from 97.5 to 103.0% and from 97.6 to 102.0% for colorimetric and photothermometric method, respectively, suggesting that our proposed color and temperature readout-based testing strategy exhibits a good accuracy and reliability, further confirming that our developed colorimetric and photothermometric method has a great potential for sensing AAO in real samples.

Conclusions

In conclusion, we explored a photothermometric sensing platform to sense AAO activity based on the redox reaction-controlled nanoprobe conversion of Prussian blue to Prussian white (PB-to-PW). The quantitative detection could be easily achieved by using a common thermometer as the simple reader. On the basis of the specific enzymatic catalytic reaction between AAO and AA as well as the unique reaction between AA and PB NPs, PB NP nanoprobe exhibited robust temperature response to the AAO analyte with high sensitivity and selectivity. More significantly, with the advantages of low cost, portability, wide availability, and simple operation, this proposed photothermometric method will bring a new horizon on the exploitation of PB NP nanoprobe-based photothermometric POCT methods.

Supplementary Information The online version contains supplementary material available at https://doi.org/10.1007/s00216-021-03629-5.

Funding This work received financial support from the National Natural Science Foundation of China (21765013, 22064014), the Key Talent Project of Gansu Province (2019-115), the Feitian Scholar Program of Gansu Province, and the Opening Project of State Key Laboratory of Bioelectronics (No. Sklb2021p11).

Declarations

Ethics approval and consent to participate We state that all the experiments related to the human serum were performed in accordance with the guidelines on administration of our lab, and approved by the ethics committee at Northwest Normal University. Study participants were fully informed regarding the purposes of the study and consent was obtained.

Conflict of interest The authors declare no competing interests.

References

1. Chen H, Liu Y, Li H, Zhang Y, Yao S. Non-oxidation reduction strategy for highly selective detection of ascorbic acid with dual-ratio fluorescence and colorimetric signals. Sensors Actuators B Chem. 2019;281:983–8. https://doi.org/10.1016/j.snb.2018.11.020.
2. Wu Z, Nan D, Yang H, Pan S, Liu H, Hu X. A ratiometric fluorescence-scattered light strategy based on MoS_2 quantum dots/CoOOH nanoflakes system for ascorbic acid detection. Anal Chim Acta. 2019;1091:59–68. https://doi.org/10.1016/j.aca.2019.09.054.
3. Ganiga M, Cyriac J. An ascorbic acid sensor based on cadmium sulphide quantum dots. Anal Bioanal Chem. 2016;408(14):3699–706. https://doi.org/10.1007/s00216-016-9454-7.
4. Ji D, Du Y, Meng H, Zhang L, Huang Z, Hu Y, Li J, Yu F, Li Z. A novel colorimetric strategy for sensitive and rapid sensing of ascorbic acid using cobalt oxyhydroxide nanoflakes and 3,3′,5,5′-tetramethylbenzidine. Sensors Actuators B Chem. 2018;256:512–9. https://doi.org/10.1016/j.snb.2017.10.070.
5. Kalaiyarasan G, Joseph J. Efficient dual-mode colorimetric/fluorometric sensor for the detection of copper ions and vitamin C based on pH-sensitive amino-terminated nitrogen-doped carbon quantum dots: effect of reactive oxygen species and antioxidants. Anal Bioanal Chem. 2019;411(12):2619–33. https://doi.org/10.1007/s00216-019-01710-8.
6. Liu J, Wang L, Bao H. A novel fluorescent probe for ascorbic acid based on seed-mediated growth of silver nanoparticles quenching of carbon dots fluorescence. Anal Bioanal Chem. 2019;411(4):877–83. https://doi.org/10.1007/s00216-018-1505-9.
7. Arrigoni R, Arrigoni O. Multicopper oxidases: an innovative approach for oxygen management of aerobic organisms. Rend Fis Acc Lincei. 2009;21(1):71–80. https://doi.org/10.1007/s12210-009-0071-7.
8. Wang B, Cao J, Dong Y, Liu F, Fu X, Ren S, Ma S, Liu Y. An in situ electron donor consumption strategy for photoelectrochemical biosensing of proteins based on ternary $Bi_2S_3/Ag_2S/TiO_2$ NT arrays. Chem Commun. 2018;54(7):806–9. https://doi.org/10.1039/c7cc08132d.
9. Luo J, Liang D, Li X, Liu S, Deng L, Ma F, Wang Z, Yang M, Chen X. Photoelectrochemical detection of human epidermal growth factor receptor 2 (HER2) based on Co_3O_4-ascorbic acid oxidase as multiple signal amplifier. Microchim Acta. 2021;188(5):166. https://doi.org/10.1007/s00604-021-04829-7.
10. Wang M, Wang M, Wang G, Su X. A fluorescence "off-on-off" sensing platform based on bimetallic gold/silver nanoclusters for ascorbate oxidase activity monitoring. Analyst. 2020;145(3):1001–7. https://doi.org/10.1039/c9an02108f.
11. Liu S, Pang S. A dual-model strategy for fluorometric determination of ascorbic acid and of ascorbic acid oxidase activity by using DNA-templated gold-silver nanoclusters. Microchim Acta. 2018;185(9):426. https://doi.org/10.1007/s00604-018-2954-8.
12. Li N, Zhang F, Sun W, Zhang L, Su X. Redox reaction-modulated fluorescence biosensor for ascorbic acid oxidase assay by using MoS_2 quantum dots as fluorescence probe. Talanta. 2021;222:121522. https://doi.org/10.1016/j.talanta.2020.121522.
13. Han X, Chen Z, Fan Q, Li K, Mu F, Luo Q, Jin Z, Shi G, Zhang M. Manganese(II)-doped zinc/germanium oxide nanoparticles as a viable fluorescent probe for visual and time-resolved fluorometric determination of ascorbic acid and its oxidase. Microchim Acta. 2019;186(7):466. https://doi.org/10.1007/s00604-019-3580-9.
14. Fu G, Sanjay ST, Zhou W, Brekken RA, Kirken RA, Li X. Exploration of nanoparticle-mediated photothermal effect of TMB-H_2O_2 colorimetric system and its application in a visual quantitative photothermal immunoassay. Anal Chem. 2018;90(9):5930–7. https://doi.org/10.1021/acs.analchem.8b00842.
15. Liu X, Zou L, Yang X, Wang Q, Zheng Y, Geng X, Liao G, Nie W, Wang K. Point-of-care assay of alkaline phosphatase enzymatic activity using a thermometer or temperature discoloration sticker as readout. Anal Chem. 2019;91(12):7943–9. https://doi.org/10.1021/acs.analchem.9b01883.
16. He S, Hai J, Sun S, Lu S, Wang B. Palladium coordination polymers nanosheets: new strategy for sensitive photothermal detection of H_2S. Anal Chem. 2019;91(16):10823–9. https://doi.org/10.1021/acs.analchem.9b02468.
17. Liu D, Tu Q, Han Y, Wang X, Kang Q, Wang P, Guo W. A dual-modal colorimetric and photothermal assay for glutathione based on MnO2 nanosheets synthesized with eco-friendly materials. Anal Bioanal Chem. 2020;412(30):8443–50. https://doi.org/10.1007/s00216-020-02982-1.
18. Tao Y, Luo F, Lin Y, Dong N, Li C, Lin Z. Quantitative gold nanorods based photothermal biosensor for glucose using a thermometer as readout. Talanta. 2021;230:122364. https://doi.org/10.1016/j.talanta.2021.122364.
19. Lu D, Jiang H, Zhang G, Luo Q, Zhao Q, Shi X. An in situ generated Prussian blue nanoparticle-mediated multimode nanozyme-linked immunosorbent assay for the detection of aflatoxin B1. ACS Appl Mater Interfaces. 2021;13(22):25738–47. https://doi.org/10.1021/acsami.1c04751.
20. Zhou W, Hu K, Kwee S, Tang L, Wang Z, Xia J, Li X. Gold nanoparticle aggregation-induced quantitative photothermal biosensing using a thermometer: a simple and universal biosensing platform. Anal Chem. 2020;92(3):2739–47. https://doi.org/10.1021/acs.analchem.9b04996.
21. Tao Y, Wang W, Fu C, Luo F, Guo L, Qiu B, Lin Z. Sensitive biosensor for p53 DNA sequence based on the photothermal effect of gold nanoparticles and the signal amplification of locked nucleic acid functionalized DNA walkers using a thermometer as readout. Talanta. 2020;220:121398. https://doi.org/10.1016/j.talanta.2020.121398.
22. Du S, Wang Y, Liu Z, Xu Z, Zhang H. A portable immune-thermometer assay based on the photothermal effect of graphene oxides for the rapid detection of Salmonella typhimurium. Biosens Bioelectron. 2019;144:111670. https://doi.org/10.1016/j.bios.2019.111670.
23. Cai G, Yu Z, Tong P, Tang D. Ti_3C_2 MXene quantum dot-encapsulated liposomes for photothermal immunoassays using a portable near-infrared imaging camera on a smartphone. Nanoscale. 2019;11(33):15659–67. https://doi.org/10.1039/c9nr05797h.

24. Li X, Yang L, Men C, Xie Y, Liu J, Zou H, Li Y, Zhan L, Huang C. Photothermal soft nanoballs developed by loading plasmonic $Cu_{2-x}Se$ nanocrystals into liposomes for photothermal immunoassay of aflatoxin B1. Anal Chem. 2019;91(7):4444–50. https://doi.org/10.1021/acs.analchem.8b05031.
25. Lv S, Zhang K, Tang D. A new visual immunoassay for prostate-specific antigen using near-infrared excited Cu_xS nanocrystals and imaging on a smartphone. Analyst. 2019;144(12):3716–20. https://doi.org/10.1039/c9an00724e.
26. Zhang K, Zhou X, Xue X, Luo M, Liu X, Xue Z. Photothermometric analysis of bismuth ions using aggregation-induced nanozyme system with a target-triggered surface cleaning effect. Anal Bioanal Chem. 2021;413(14):3655–65. https://doi.org/10.1007/s00216-021-03312-9.
27. Huang L, Yu Z, Chen J, Tang D. Pressure-based bioassay perceived by a flexible pressure sensor with synergistic enhancement of the photothermal effect. ACS App Bio Mater. 2020;3(12):9156–63. https://doi.org/10.1021/acsabm.0c01447.
28. Fu G, Sanjay ST, Dou M, Li X. Nanoparticle-mediated photothermal effect enables a new method for quantitative biochemical analysis using a thermometer. Nanoscale. 2016;8(10):5422–7. https://doi.org/10.1039/c5nr09051b.
29. Wei Y, Wang D, Zhang Y, Sui J, Xu Z. Multicolor and photothermal dual-readout biosensor for visual detection of prostate specific antigen. Biosens Bioelectron. 2019;140:111345. https://doi.org/10.1016/j.bios.2019.111345.
30. Hong G, Zhang D, He Y, Yang Y, Chen P, Yang H, Zhou Z, Liu Y, Wang Y. New photothermal immunoassay of human chorionic gonadotropin using Prussian blue nanoparticle-based photothermal conversion. Anal Bioanal Chem. 2019;411(26):6837–45. https://doi.org/10.1007/s00216-019-02049-w.
31. Peng X, Wang R, Wang T, Yang W, Wang H, Gu W, Ye L. Carbon dots/Prussian blue satellite/core nanocomposites for optical imaging and photothermal therapy. ACS Appl Mater Interfaces. 2018;10(1):1084–92. https://doi.org/10.1021/acsami.7b14972.
32. Guo L, Zhang Y, Yu Y, Wang J. In situ generation of Prussian blue by MIL-53 (Fe) for point-of-care testing of butyrylcholinesterase activity using a portable high-throughput photothermal device. Anal Chem. 2020;92(21):14806–13. https://doi.org/10.1021/acs.analchem.0c03575.
33. Fu G, Liu W, Feng S, Yue X. Prussian blue nanoparticles operate as a new generation of photothermal ablation agents for cancer therapy. Chem Commun. 2012;48(94):11567–9. https://doi.org/10.1039/c2cc36456e.
34. Fu G, Zhu Y, Xu K, Wang W, Hou R, Li X. Photothermal microfluidic sensing platform using near-infrared laser-driven multiplexed dual-mode visual quantitative readout. Anal Chem. 2019;91(20):13290–6. https://doi.org/10.1021/acs.analchem.9b04059.
35. Xue X, Gao M, Rao H, Luo M, Wang H, An P, Feng T, Lu X, Xue Z, Liu X. Photothermal and colorimetric dual mode detection of nanomolar ferric ions in environmental sample based on in situ generation of prussian blue nanoparticles. Anal Chim Acta. 2020;1105:197–207. https://doi.org/10.1016/j.aca.2020.01.049.
36. Cheng M, Peng W, Hua P, Chen Z, Sheng J, Yang J, Wu Y. In situ formation of pH-responsive Prussian blue for photoacoustic imaging and photothermal therapy of cancer. RSC Adv. 2017;7(30):18270–6. https://doi.org/10.1039/c7ra01879g.
37. Han X, Lin S, Li Y, Cheng C, Han X. Near-infrared photothermal immunoassay for pancreatic cancer biomarker CA 19-9 on a digital thermometer. Anal Chim Acta. 2020;1098:117–24. https://doi.org/10.1016/j.aca.2019.11.027.
38. Zhi L, Sun A, Tang D. In situ amplified photothermal immunoassay for neuron-specific enolase with enhanced sensitivity using Prussian blue nanoparticle-loaded liposomes. Analyst. 2020;145(12):4164–72. https://doi.org/10.1039/d0an00417k.
39. Farka Z, Cunderlova V, Horackova V, Pastucha M, Mikusova Z, Hlavacek A, Skladal P. Prussian blue nanoparticles as a catalytic label in a sandwich nanozyme-linked immunosorbent assay. Anal Chem. 2018;90(3):2348–54. https://doi.org/10.1021/acs.analchem.7b04883.
40. Fu G, Sanjay ST, Li X. Cost-effective and sensitive colorimetric immunosensing using an iron oxide-to-Prussian blue nanoparticle conversion strategy. Analyst. 2016;141(12):3883–9. https://doi.org/10.1039/c6an00254d.
41. Ma H, He Y, Liu H, Xu L, Li J, Huang M, Wei Y. Anchoring of Prussian blue nanoparticles on polydopamine nanospheres as an efficient peroxidase mimetic for colorimetric sensing. Colloid Surface A. 2019;577:622–9. https://doi.org/10.1016/j.colsurfa.2019.06.035.
42. Chen F, Teng L, Lu C, Zhang C, Rong Q, Zhao Y, Yang Y, Wang Y, Song G, Zhang X. Activatable magnetic/photoacoustic nanoplatform for redox-unlocked deep-tissue molecular imaging in vivo via Prussian blue nanoprobe. Anal Chem. 2020;92(19):13452–61. https://doi.org/10.1021/acs.analchem.0c02859.
43. Zloczewska A, Celebanska A, Szot K, Tomaszewska D, Opallo M, Jönsson-Niedziolka M. Self-powered biosensor for ascorbic acid with a Prussian blue electrochromic display. Biosens Bioelectron. 2014;54:455–61. https://doi.org/10.1016/j.bios.2013.11.033.
44. Granica M, Tymecki L. Prussian blue (bio) sensing device for distance-based measurements. Anal Chim Acta. 2020;1136:125–33. https://doi.org/10.1016/j.aca.2020.08.037.